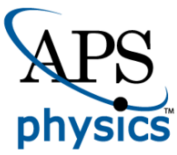

Baryon destruction by asymmetric dark matter

Hooman Davoudiasl, David E. Morrissey, Kris Sigurdson, and Sean Tulin

Phys. Rev. D **84**, 096008 — Published 10 November 2011

DOI: 10.1103/PhysRevD.84.096008

Baryon Destruction by Asymmetric Dark Matter

Hooman Davoudiasl[(a)], David E. Morrissey[(b)], Kris Sigurdson[(c)], Sean Tulin[(b)]

(a) *Department of Physics, Brookhaven National Laboratory, Upton, NY 11973, USA*

(b) *Theory Group, TRIUMF, 4004 Wesbrook Mall, Vancouver, BC V6T 2A3, Canada*

(c) *Department of Physics and Astronomy, University of British Columbia, Vancouver, BC V6T 1Z1, Canada*

email: hooman@bnl.gov, dmorri@triumf.ca, krs@physics.ubc.ca, tulin@triumf.ca

October 17, 2011

Abstract

We investigate new and unusual signals that arise in theories where dark matter is asymmetric and carries a net antibaryon number, as may occur when the dark matter abundance is linked to the baryon abundance. Antibaryonic dark matter can cause *induced nucleon decay* by annihilating visible baryons through inelastic scattering. These processes lead to an effective nucleon lifetime of $10^{29} - 10^{32}$ years in terrestrial nucleon decay experiments, if baryon number transfer between visible and dark sectors arises through new physics at the weak scale. The possibility of induced nucleon decay motivates a novel approach for direct detection of cosmic dark matter in nucleon decay experiments. Monojet searches (and related signatures) at hadron colliders also provide a complementary probe of weak-scale dark-matter–induced baryon number violation. Finally, we discuss the effects of baryon-destroying dark matter on stellar systems and show that it can be consistent with existing observations.

1 Introduction

Cosmological observations indicate that about 4.6% of the energy density of the Universe consists of baryonic matter, while 23% is dark matter (DM) [1]. Neither of these results can be explained with our current understanding of elementary particles, the standard model (SM). Cosmology therefore requires new fundamental physics, and it is important to find ways to detect such new physics experimentally.

In the majority of new-physics scenarios, the generation of baryons and DM occurs through unrelated mechanisms, offering no explanation for the similar magnitudes of their cosmological densities. The most thoroughly studied scenarios involve baryon production from CP-violating non-equilibrium processes during the electroweak phase transition, from decays of right-handed neutrinos, or from the coherent evolution of scalar fields [2], while the DM relic density is determined by thermal freeze out when a non-relativistic stable species falls out of equilibrium [3]. In this context, there is no reason to expect similar cosmological densities of baryons and DM.

This apparent coincidence may instead be a clue that both types of matter have a common origin. Several models of asymmetric dark matter (ADM) have been proposed along these lines where the DM density carries a net (approximately) conserved global charge shared by the SM [4, 5, 6, 7, 8, 9, 10, 11, 12, 13, 14, 15], such as baryon number B. These models generally fall into two classes depending on how the charge asymmetry is created:

1. An initial charge asymmetry, generated in either the visible or DM sector, is partitioned between the two sectors by chemical equilibration through a transfer operator [4, 9]. These charges are separately "frozen in" once the transfer operator goes out of equilibrium.

2. Non-equilibrium dynamics generate equal and opposite charge asymmetries in the visible and DM sectors, without any net overall charge asymmetry [10, 11, 12, 13, 14, 15]. In order to avoid washout, transfer operators must always be out of equilibrium once the asymmetries are created. We term this process *hylogenesis* ("hyle" = matter) [15].

Subsequently, in both cases, DM particles and antiparticles are assumed to annihilate efficiently, leaving only a remnant asymmetric component determined by the charge density.

In the present work, we investigate novel experimental signatures from hylogenesis scenarios where DM carries B [15]. Here, the lowest-dimensional, gauge-invariant transfer operator is given by

$$\mathscr{L}_{\text{eff}} \sim \frac{1}{\Lambda^3}\, u_R^i d_R^j d_R^k \Psi_R \Phi + \text{h.c.} \tag{1}$$

where i, j, k label generation. In this case, DM has two components, a fermion/scalar pair (Ψ, Φ) with total baryon number $B_\Psi + B_\Phi = -1$. Stability of both Ψ and Φ requires $|m_\Psi - m_\Phi| < (m_p + m_e)$. This operator is inactive cosmologically and does not wash out the baryon-DM asymmetry for $\Lambda \gtrsim 100$ GeV provided the asymmetry is created at relatively

low temperatures, below about a GeV. Our results may also be applicable to other ADM scenarios in which the same transfer operator appears with one or both of (Ψ, Φ) making up the DM.

In hylogenesis, the Universe is net B-symmetric, and therefore the baryon asymmetry carried by DM is equal and opposite to that in visible baryons. Specifically, in the hylogensis scenario of Ref. [15], this has two important consequences:

- The number densities of (Ψ, Φ) satisfy $n_\Psi = n_\Phi = n_B$. Therefore, cosmological observations imply $(m_\Psi + m_\Phi)/m_p = \Omega_{DM}/\Omega_b \approx 5$. Together with the DM stability requirement, we have $m_{\Psi,\Phi} \approx 1.7 - 2.9$ GeV.

- There exist many scenarios in which ADM is coupled to the SM via the "neutron portal" operator $u_R d_R d_R$ [4], generally falling into the first class of "chemical equilibration" scenarios. In this case, DM is very often baryonic ($B_{DM} > 0$), while for hylogenesis scenarios the DM must be antibaryonic ($B_{DM} < 0$).[1]

In Ref. [15], we presented a specific realization for hylogenesis where the operator in Eq. (1) arises by integrating out heavy Dirac fermion mediatiors $X_{1,2}$. Out-of-equilibrium decays of X_1 during reheating generate equal-and-opposite dark and visible baryon asymmetries. Furthermore, in this scenario (Ψ, Φ) are charged under an additional hidden $U(1)'$ gauge symmetry, that couples to the SM via kinetic mixing with hypercharge, to facilitate annihilation of the symmetric DM densities. More details about this realization are given in Appendix A.

Hylogenesis models with the operator of Eq. (1) have an interesting and unique signature: antibaryonic DM particles can annihilate visible baryonic matter, termed *induced nucleon decay* (IND). IND is a novel and unusual DM signal. These events are $\Psi N \to \Phi^\dagger M$ and $\Phi N \to \bar{\Psi} M$, where $N = (n, p)$ is a nucleon and M is a meson. Since the DM states are invisible, this mimics nucleon decay, with an effective lifetime dependent on the local DM density. This signal offers the new and exciting possibility of searching for DM in nucleon decay searches in deep underground detectors such as SuperKamiokande [18].

In Section 2, we compute the rates and kinematics of IND, and discuss the implications of IND for existing nucleon decay searches. Our main conclusions are: (i) due to different kinematics of IND, compared to standard nucleon decay, existing bounds do not apply over most of the region of parameter space of our DM model, and (ii) the effective nucleon lifetime can be around $10^{29} - 10^{32}$ years, if the new physics scale Λ in Eq. (1) is the weak scale.

Hadron colliders can probe (anti)baryonic DM scenarios through direct production of the weak-scale mediators transfering B between visible and dark sectors, discussed in Section 3. The operator of Eq. (1) can give rise to observable signatures in the form of monojets (or jets and missing energy). Within our hylogenesis model, if IND were detected in nucleon decay searches, monojet signals are inescapable and should be observed at the Large Hadron Collider (LHC).

[1] In supersymmetric models, light superpartners can play an important role in chemical equilibration [16], potentially affecting the sign of B_{DM} in equilibration ADM scenarios. Also, for other applications of the neutron portal operator to baryogenesis, see Ref. [17].

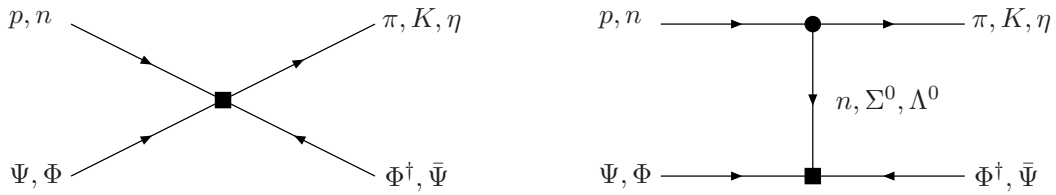

Figure 1: *Feynman diagrams for induced nucleon decay. Box denotes IND vertex from Eq.* (9). *Circle denotes strong interaction vertex given by* $\mathscr{L}_0$ *in Ref. [23].*

IND processes can potentially be relevant in stars. Since the IND rate scales with the DM density, capture and accretion of DM in stars is important, possibly leading to modification of stellar evolution due to baryon destruction and energy injection. In Section 4, we consider these effects in neutron stars, white dwarfs, and main-sequence stars. Our conclusions are summarized in Section 5.

2 Dark Matter Detection in Nucleon Decay Searches

Dark matter particles (Ψ, Φ) can annihilate nucleons N, producing an energetic meson M through inelastic scattering

$$\Phi N \longrightarrow \bar{\Psi} M \,, \qquad \Psi N \longrightarrow \Phi^\dagger M \,, \tag{2}$$

shown in Figure 1. We restrict our attention to single meson final states, although multi-meson events are allowed and may have comparable rates. In general, both down-scattering and up-scattering can occur, defined as whether the heavier or lighter DM particle, respectively, is in the initial state; however, the latter is kinematically forbidden if $|m_\Psi - m_\Phi| > m_N - m_M$. Since neither the initial DM nor final anti-DM particles are observed directly, these processes mimic standard nucleon decay events $N \to M\nu$ [19], with an undetected final state neutrino ν (or antineutrino $\bar{\nu}$).

The observable meson energy for each case in Eq. (2) is, respectively,

$$E_M = \frac{(m_N + m_\Phi)^2 + m_M^2 - m_\Psi^2}{2(m_N + m_\Phi)} \,, \quad E_M = \frac{(m_N + m_\Psi)^2 + m_M^2 - m_\Phi^2}{2(m_N + m_\Psi)} \,, \tag{3}$$

neglecting the initial kinetic energy of the DM particles ($v_{DM} \sim 10^{-3}$).

Although hylogenesis (as a baryogenesis mechanism) works for any quark flavor, the most interesting signatures arise if the IND operators involve u, d, s quarks only. Restricting our attention to the lightest mesons (π, K, η), the final state meson can have much more kinetic energy in IND than for standard nucleon decay (SND), summarized in Table. 1. For fixed masses m_Ψ and m_Φ, the meson is either monochromatic or bichromatic (up to Fermi motion), depending on whether up-scattering is forbidden or allowed. The range of momenta p_M corresponds to the allowed range $m_{\Psi,\Phi} \approx 2 - 3$ GeV, provided that (Ψ, Φ) are stable and account for the observed Ω_{DM}.

Decay mode	p_M^{SND}	p_M^{IND} [up]	p_M^{IND} [down]	τ_N^{SND} bound ($\times 10^{32}$ yr)
$N \to \pi$	460	< 800	$800 - 1400$	$\tau_p^{SND} > 0.16$ [20] , $\tau_n^{SND} > 1.12$ [21]
$N \to K$	340	< 680	$680 - 1360$	$\tau_p^{SND} > 23$ [18] , $\tau_n^{SND} > 1.3$ [18]
$N \to \eta$	310	< 650	$650 - 1340$	$\tau_n^{SND} > 1.58$ [21]

Table 1: *Comparison of meson $M = (\pi, K, \eta)$ momentum p_M (MeV) for standard nucleon decay (SND) and induced nucleon decay (IND) from DM, for up- and down-scattering.*

2.1 Nucleon decay searches

Existing searches have been optimized for meson momenta $p_M^{SND} \sim 300 - 450$ MeV, while for IND mesons are typically much more energetic, with momenta $p_M^{IND} \sim 1$ GeV. Here, we briefly summarize existing SND search strategies and how they might be adapted for IND searches.

$\underline{p \to K^+\nu,\ n \to K^0\nu}$**:** The Super-Kamiokande experiment, a water Čerenkov detector, provides the strongest limits on these channels. For K^+, they have three searches: (*i*) $K^+ \to \pi^+\pi^0$, giving three Čerenkov rings, (*ii*) $K^+ \to \mu^+$ with a prompt γ (from $^{16}\mathrm{O} \to {}^{15}\mathrm{N}^* \to {}^{15}\mathrm{N} + \gamma$), and (*iii*) a mono-energetic μ^+ from $K^+ \to \mu^+$, with no prompt γ. All three searches assume, as is the case for $p_{K^+} \approx 340$ in SND, that the K^+ is emitted below Čerenkov threshold ($\beta < 0.75$) and comes to rest before decaying. For IND, we estimate that an $\mathcal{O}(1)$ fraction of K^+'s do come to rest before decaying. However, except for up-scattering events close to kinematic threshold, the K^+ from IND has $\beta > 0.75$, adding an extra ring to the event topology. Furthermore, this additional radiation may make finding the prompt γ in search method (*ii*) more difficult. For K^0, they have two searches: (*iv*) $K_S^0 \to \pi^0\pi^0 \to 4\gamma$, giving four e-like rings, and (*v*) $K_S^0 \to \pi^+\pi^-$, giving two μ-like rings. Both searches assume $200 < p_{K^0} < 500$ MeV, thereby excluding IND events (again, except for up-scattering near kinematic threshold). One difficulty in search (*iv*) is identifying all four e-like rings. For IND, this may be more difficult as the rings would be more overlapping due to relativistic beaming. On the other hand, search (*v*) is promising for IND. In SND this mode suffers from a small efficiency that the $\pi^\pm$ are both above Čerenkov threshold. With greater energetics in IND, the efficiency may be much larger.

$\underline{p \to \pi^+\nu}$**:** The best limit is provided by the Soudan 2 experiment, an iron tracking calorimeter. Nucleon decay event candidates were required to have a single π^+ track, with ionization consistent with mass m_π or m_μ, initial momentum $140 < p_{\pi^+} < 420$ MeV, and visible endpoint decays ($\pi^+ \to \mu^+ \to e^+$). Their simulations showed that a π^+ originating from within an iron nucleus loses on average half its initial momentum. At higher p_{π^+}, IND events may be more visible due to reduced background from atmospheric neutrinos. However, it is unknown to us what is the average momentum deposition in iron of the π^+ at much higher energy, and whether this can lead to fragmentation of the parent nucleus into exotic nuclear states.

$\underline{n \to \pi^0\nu,\ n \to \eta\nu}$**:** The best limits on these modes come from the IMB-3 experiment, a

water Čerenkov detector.[2] The $\pi^0 \to \gamma\gamma$ channel may be more difficult at higher energies: due to decreased separation angle of the two photons (from relativistic beaming), they can appear as a single electron-like track. The $n \to \eta\nu,\ \eta \to \gamma\gamma$ channel will have greater photon separation and may be more promising. We find that the IND rates into π^0 and η final states are comparable and are sensitive to the same underlying IND operator (shown below).

2.2 Effective nucleon lifetime from IND

An effective IND lifetime can be defined as the inverse scattering rate per target nucleon, $\tau_N^{-1} \equiv n_{DM}(\sigma v)_{IND}$, with local DM number density $n_{DM} \equiv \rho_{DM}/(m_\Psi + m_\Phi)$ and IND scattering cross section $(\sigma v)_{IND}$. Numerically, we have

$$\tau_N^{-1} \approx (10^{32}\ \text{yrs})^{-1} \times \left(\frac{\rho_{DM}}{0.3\,\text{GeV/cm}^3}\right)\left(\frac{(\sigma v)_{IND}}{10^{-39}\,\text{cm}^3/\text{s}}\right) . \tag{4}$$

Next, we compute $(\sigma v)_{IND}$ using chiral perturbation theory. We perform an expansion in powers of $p_M/(4\pi f)$, where $f \approx 139$ MeV is the pion decay constant, and truncate at leading order. Since for IND we expect $p_M \sim 4\pi f \sim 1$ GeV, our calculations should be regarded as order-of-magnitude estimates at best. Our analysis closely follows SND rate computations in Ref. [23].

There are four effective interactions that are relevant for IND processes with single meson final states. These are given by $\mathscr{L}_{\rm int} = \sum_i c_i O_i$, with operators (given in two-component spinor notation)

$$O_1 = \epsilon_{\alpha\beta\gamma}\Phi(u_R^\alpha d_R^\beta)(d_R^\gamma \Psi_R) \tag{5}$$

$$O_2 = \frac{1}{\sqrt{6}}\,\epsilon_{\alpha\beta\gamma}\Phi[(d_R^\alpha s_R^\beta)(u_R^\gamma\Psi_R) + (s_R^\alpha u_R^\beta)(d_R^\gamma\Psi_R) - 2(u_R^\alpha d_R^\beta)(s_R^\gamma\Psi_R)] \tag{6}$$

$$O_3 = \frac{1}{\sqrt{2}}\,\epsilon_{\alpha\beta\gamma}\Phi[(d_R^\alpha s_R^\beta)(u_R^\gamma\Psi_R) - (s_R^\alpha u_R^\beta)(d_R^\gamma\Psi_R)] \tag{7}$$

where α, β, γ are color indices, and the coefficients c_i have mass dimension -3.[3] The linear combinations have been chosen such that $O_{1,2,3}$ have strong isospin $I = (\frac{1}{2},\, 0,\, 1)$, respectively. Here, it is useful to write $\mathscr{L}_{\rm int} = \text{Tr}(c\,O)$ where

$$c \equiv \begin{pmatrix} \frac{c_2}{\sqrt{6}} + \frac{c_3}{\sqrt{2}} & 0 & 0 \\ 0 & \frac{c_2}{\sqrt{6}} - \frac{c_3}{\sqrt{2}} & 0 \\ 0 & c_1 & -\sqrt{\frac{2}{3}}\,c_2 \end{pmatrix} , \quad O_{ij} \equiv \frac{1}{2}\,\epsilon_{\alpha\beta\gamma}\,\epsilon_{jk\ell}\,(q_{Rk}^\alpha q_{R\ell}^\beta)(q_{iR}^\gamma\Psi_R)\Phi\ , \tag{8}$$

[2] We note that the IMB-3 experiment found an excess in events with total energy $900 - 1100$ MeV (20 events vs. 6.1 expected background) [22]. Nearly all these events had between $2 - 4$ Čerenkov rings, large missing momenta ($400 - 1100$ MeV), and large invariant masses ($600 - 1100$ MeV). In IND, a large missing momentum would be expected, while a large invariant mass could arise through heavy meson or multi-meson final states.

[3] A fourth operator $\epsilon_{\alpha\beta\gamma}\Phi(s_R u_R)(s_R\Psi_R)$ is relevant only for multi-kaon final states. A fifth operator $\epsilon_{\alpha\beta\gamma}\Phi[(d_R^\alpha s_R^\beta)(u_R^\gamma\Psi_R) + (s_R^\alpha u_R^\beta)(d_R^\gamma\Psi_R) + (u_R^\alpha d_R^\beta)(s_R^\gamma\Psi_R)]$ vanishes by a Fierz identity.

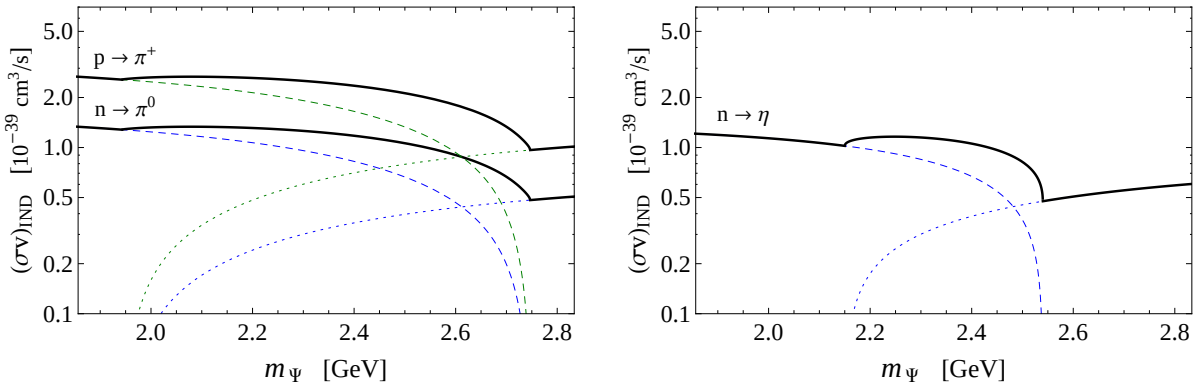

Figure 2: *Induced nucleon decay cross sections* $(\sigma v)_{IND}$ *for* $p, n \to \pi^+, \pi^0$ *(left) and* $n \to \eta$ *(right) as a function of fermion DM mass* m_Ψ *for* $|c_1| = TeV^{-3}$*. Dotted (dashed) lines denote* $N\Phi \to \bar{\Psi} M$ *(*$N\Psi \to \Phi^\dagger M$*). Solid lines denote total rates* $N\Phi \to \bar{\Psi} M + N\Psi \to \Phi^\dagger M$*.* $(\sigma v)_{IND} = 10^{-39}\ cm^3/s$ *corresponds to lifetime* $\tau_N^{IND} = 10^{32}$ *years.*

with $q_R^\alpha \equiv (u, d, s)_R^\alpha$. Under $SU(3)_L \times SU(3)_R$ chiral symmetry transformations, the right-handed quark fields transform in the $(\mathbf{1}, \mathbf{3})$ representation, $q_R \to R\, q_R$ (where $R \in SU(3)_R$), while the IND operator O_{ij} transforms in the $(\mathbf{1}, \mathbf{8})$ representation, $O \to ROR^\dagger$. If we treat c as a spurion in the $(\mathbf{1}, \mathbf{8})$ representation, $\mathscr{L}_{\rm int}$ is invariant under chiral transformations. (The DM fields (Ψ, Φ) are chiral singlets.)

The IND interactions of baryon and (pseudo-Goldstone) meson fields are determined by the chiral transformation properties of the spurion c. Following the conventions of Ref. [23], the only invariant operator is

$$\mathscr{L}_{IND} = \beta\, \mathrm{Tr}[c\, \xi^\dagger (B_R \Psi_R) \Phi \xi] \ , \tag{9}$$

where $\xi \equiv \exp(iM/f)$. The meson and baryon fields are

$$M = \begin{pmatrix} \frac{\eta}{\sqrt{6}} + \frac{\pi^0}{\sqrt{2}} & \pi^+ & K^+ \\ \pi^- & \frac{\eta}{\sqrt{6}} - \frac{\pi^0}{\sqrt{2}} & K^0 \\ K^- & \bar{K}^0 & -\sqrt{\frac{2}{3}}\,\eta \end{pmatrix} , \quad B = \begin{pmatrix} \frac{\Lambda^0}{\sqrt{6}} + \frac{\Sigma^0}{\sqrt{2}} & \Sigma^+ & p \\ \Sigma^- & \frac{\Lambda^0}{\sqrt{6}} - \frac{\Sigma^0}{\sqrt{2}} & n \\ \Xi^- & \Xi^0 & -\sqrt{\frac{2}{3}}\,\Lambda^0 \end{pmatrix} . \tag{10}$$

Eq. (9) is invariant since the quantity $(\xi^\dagger B_R \xi)$ is in the $(\mathbf{1}, \mathbf{8})$ representation [23]. The unknown overall coefficient $\beta = 0.014(1)$ GeV^3 has been computed using lattice methods [24].

The Feynman diagrams for IND are given in Fig. 1. It is straight-forward to derive the Feynman rules for the interactions of baryons, mesons, and DM by expanding the matrix expressions in Eq. (9) and working to linear order in $1/f$. From these, we compute the matrix elements and cross sections for IND processes. We assume that only one coefficient c_i is non-zero at a time. $N \to \pi, \eta$ modes depend only on c_1, while $N \to K$ modes are governed by $c_{2,3}$.

Our numerical results are shown in Figs. 2 and 3, for the five decay modes we consider. We plot the velocity-weighted cross sections $(\sigma v)_{IND}$ for each mode, as a function of $m_\Psi \approx$

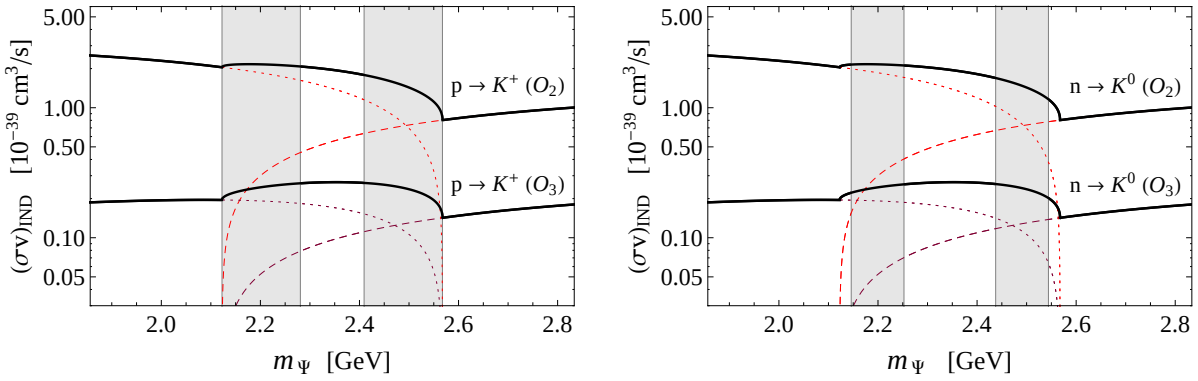

Figure 3: *Induced nucleon decay cross sections $(\sigma v)_{IND}$ for $p \to K^+$ (left) and $n \to K^0$ (right) as a function of fermion DM mass m_Ψ for $|c_{2,3}| = TeV^{-3}$. Dotted (dashed) lines denote $N\Phi \to \bar{\Psi}K$ ($N\Psi \to \Phi^\dagger K$) from operators $O_{2,3}$. Solid lines denote total rates $N\Phi \to \bar{\Psi}K + N\Psi \to \Phi^\dagger K$. Grey regions show where existing nucleon decay bounds apply, described in text.*

$(5m_p - m_\Phi)$, for the allowed range $2m_p < m_\Psi < 3m_p$ (as required by DM stability). In Fig. 2, the solid lines show the total cross sections for the channels $p \to \pi^+$ and $n \to \pi^0$ (left) and $n \to \eta$ (right). All three modes arise from the same IND operator O_1, and we have fixed $c_1 = \text{TeV}^{-3}$. The individual cross sections for $N\Psi \to M\Phi^\dagger$ ($N\Phi \to M\bar{\Psi}$) are shown by the dotted (dashed) curves. Although the individual rates vanish where kinematically forbidden, the total rate is always non-vanishing. For $|m_\Psi - m_\Phi| < m_N - m_M$, both up- and down-scattering rates are non-zero, and IND is bichromatic. Otherwise, only down-scattering is allowed, and IND is monochromatic.

In Fig. 3, we show the strange IND channels $p \to K^+$ (left) and $n \to K^0$ (right). Here, there are two relevant operators $O_{2,3}$. The solid lines denote the total IND cross sections induced by each O_i independently, taking $c_i = \text{TeV}^{-3}$, for $i = 2, 3$. The individual cross sections for $N\Psi \to M\Phi^\dagger$ ($N\Phi \to M\bar{\Psi}$) are shown by the dotted (dashed) curves. Again, the kaons can be monochromatic or bichromatic, depending on whether up-scattering is kinematically allowed.

Existing nucleon decay bounds do apply in select regions of parameter space for up-scattering close to threshold, where the meson momentum is reduced. We illustrate these regions in Fig. 3, shown in grey, for the case of Super-Kamiokande. For $p \to K^+$, this region corresponds to $\beta_{K^+} < 0.75$: in this case, the K^+ is below Čerenkov threshold and the event topology is identical to $p \to K^+\nu$. For $n \to K^0$, this region corresponds to a kinematic window $200 < p_{K^0} < 500$ MeV, as in their $n \to K^0\nu$ search. We emphasize that Super-Kamiokande bounds constrain only the up-scattering IND rate, which can be suppressed compared to down-scattering in these parameter regions.

The total IND rate depends sensitively on the unknown mass scale $\Lambda_{IND} \equiv |c_i|^{-1/3}$. The total IND cross sections and nucleon lifetimes for all channels are comparable, scaling as

$$(\sigma v)_{IND} \approx 10^{-39}\ \text{cm}^3/\text{s} \times \left(\frac{\Lambda_{IND}}{1\ \text{TeV}}\right)^{-6}, \quad \tau_N \approx 10^{32}\ \text{yr} \times \left(\frac{\Lambda_{IND}}{1\ \text{TeV}}\right)^{6} \left(\frac{\rho_{DM}}{0.3\ \text{GeV/cm}^3}\right). \quad (11)$$

As we show in Sec. 3, the collider bound on this scale is $\Lambda_{IND} \gtrsim 300$ GeV. Therefore, τ_N can in principle be as low as 10^{29} years. It is likely that such a short lifetime would be excluded from nucleon decay searches, but no dedicated IND search has yet been performed. We also note that future nucleon decay experiments are envisioned to have markedly better reach for τ_N. For example, a water Čerenkov detector with 10^4 kton $\times$ year of exposure can reach $\tau_N \sim 10^{(34-35)}$ yr [25, 26]; a similar capability is expected to be achieved with a liquid Argon detector with 10^3 kton $\times$ year of exposure [27]. For kaon final states, liquid Argon technology is expected to provide improved efficiency due to better imaging capabilities [27].

Lastly, we note that the IND cross sections satisfy certain relations, as a consequence of strong isospin symmetry:

$$(\sigma v)_{IND}^{p\to\pi^+} = 2\,(\sigma v)_{IND}^{n\to\pi^0}\,, \quad (\sigma v)_{IND}^{p\to K^+} = (\sigma v)_{IND}^{n\to K^0}\,. \tag{12}$$

The latter relation holds only if $N \to K$ modes are dominated by either O_2 or O_3, as assumed in Fig. 3. If neither operator is negligible, then $(\sigma v)_{IND}^{p\to K^+} \neq (\sigma v)_{IND}^{n\to K^0}$. In this case, both K modes are complementary and can be used to disentangle the underlying IND operator structure.

3 Collider Signals from Hylogenesis

ADM scenarios rely on transfer operators to connect global charge between the visible and dark sectors, and these operators can be probed at high-energy colliders. In the specific hylogenesis model of Ref. [15], B is mediated between the two sectors by heavy Dirac fermions $X_{1,2}$ ($m_{X_1} < m_{X_2}$), through interactions of the form

$$-\mathscr{L} \supset \sum_{a=1,2} \frac{\lambda_a^{ijk}}{M^2}\,(u_R^i d_R^j)(X_{a,L}^\dagger d_R^k) + \zeta_a\,(X_{a,L}\Psi_L + X_{a,R}\Psi_R)\Phi + \text{h.c.} \tag{13}$$

where i, j, k label generation, color indices are implicitly contracted antisymmetrically, and other fermion contractions are also possible. Integrating out $X_{1,2}$ generates operators of the form of Eq. (1).

The $X_{1,2}$ particles can be produced at high-energy hadron colliders through the operator of Eq. (13). With decays $X_{1,2} \to \bar{\Psi}\Phi^\dagger$, this gives rise to events involving missing energy and one or more jets. In this section, we investigate the sensitivity of the Tevatron and the LHC to such events and we derive a corresponding bound on the heavy mass scale M suppressing the neutron portal operator. Related studies in the context of WIMP and other dark matter candidates can be found in Refs. [28, 29, 30, 31, 32, 33].

To be concrete, we will focus on the lighter state $X_1 \equiv X$, with the specific interaction

$$-\mathscr{L} \;\supset\; \frac{\lambda}{M^2}(X_L^\dagger s_R)(u_R d_R) + \zeta\, X\Psi\Phi + h.c., \tag{14}$$

We expect other flavour structures and fermion contractions to give qualitatively similar results. The operator of Eq. (14) can give rise to processes of the form

$$q(p_1)\,q'(p_2) \;\to\; \bar{q}''(p_3)\,\bar{\Psi}(p_4)\,\Phi^\dagger(p_5) \tag{15}$$

through either a real or off-shell X, where $q, q', q'' = u, d, s$ quarks. The corresponding summed and averaged squared matrix element can take two possible forms, depending on how the fermions are contracted. They are:

$$|\mathcal{M}|^2 = \begin{cases} \frac{2}{3}\left|\frac{\lambda\zeta}{M^2}\right|^2 \left|\frac{1}{q^2-m_x^2+i\Gamma_x m_x}\right|^2 (p_1\cdot p_2)\left[2(p_3\cdot q)(p_4\cdot q)-(q^2-m_X^2)(p_3\cdot p_4)\right] \ ; & s\text{-like} \\ \frac{2}{3}\left|\frac{\lambda\zeta}{M^2}\right|^2 \left|\frac{m_x}{q^2-m_x^2+i\Gamma_x m_x}\right|^2 (p_1\cdot p_3)\left[2(p_2\cdot q)(p_4\cdot q)-(q^2-m_X^2)(p_2\cdot p_4)\right] \ ; & t\text{-like} \end{cases} \tag{16}$$

Here, $q = (p_4+p_5) = (p_1+p_2-p_3)$ is the momentum carried by the intermediate X state, and $\Gamma_x = \zeta^2 m_X/16\pi$ is the width of the X state which we assume decays mainly into $\bar{\Psi}\Phi^\dagger$. The s-like form correponds to the case where both initial state fermions are contracted together in the underlying operator while the t-like form corresponds to a contraction between initial and final state quarks.

At the Tevatron and the LHC, we find that the full cross section derived from the matrix elements of Eq. (16) is frequently dominated by the pole in the intermediate X propagator. This corresponds to the production of an on-shell X state whose mass is not much smaller than the higher-dimensional operator scale M, and corresponds to a large momentum transfer.[4] In this case the higher-dimensional operator structures we are using become unreliable and the full dynamics of the unknown ultraviolet completion becomes relevant. Without specifying the underlying theory, we can still parametrize the generic behaviour in a reasonable way as follows. For s-like contractions, whose structure would arise most naturally from a boson in the s-channel, we make the replacement

$$\frac{\lambda}{M^2} \to \frac{\lambda}{\hat{s} - M^2 + i\sqrt{\hat{s}}\Gamma}, \tag{17}$$

where $\hat{s}$ is the parton-level Mandelstam variable and Γ is the decay width of the mediator. In the absence of an underlying theory, we parametrize this quantity as $\Gamma = \mathcal{C}M$ and consider the values $\mathcal{C} = 1/5,\ 1/50$. For t-like contractions, we make the replacement

$$\frac{\lambda}{M^2} \to \frac{\lambda}{\hat{t} - M^2}, \tag{18}$$

where $\hat{t} = (p_1 - p_3)^2$ is the parton-level Mandelstam variable. Since $\hat{t}$ is negative, we do not bother adding a width term.

We apply these matrix elements to compute the leading-order (LO) monojet production cross sections at the Tevatron by convolving with CTEQ6.1M parton distribution functions [34] and integrating over phase space. To match the most stringent Tevatron monojet search bounds, we impose a cut of $p_T > 80$ GeV and $|\eta| < 1.0$ on the outgoing jet. Following Ref. [30], we also apply a flat efficiency factor of 40% to connect our parton-level cross section to the full hadronic jet reconstruction at the Tevatron detectors. The cross sections computed in this way (after applying cuts and the efficiency factor) are shown in Fig. 4 for the parameter values $m_X = 0.75M,\ 1.5M$ and $\Gamma = M/5,\ M/50$. We also set $\lambda = 1$ and

[4] This is a necessary condition for hylogenesis to create a sufficiently large asymmetry.

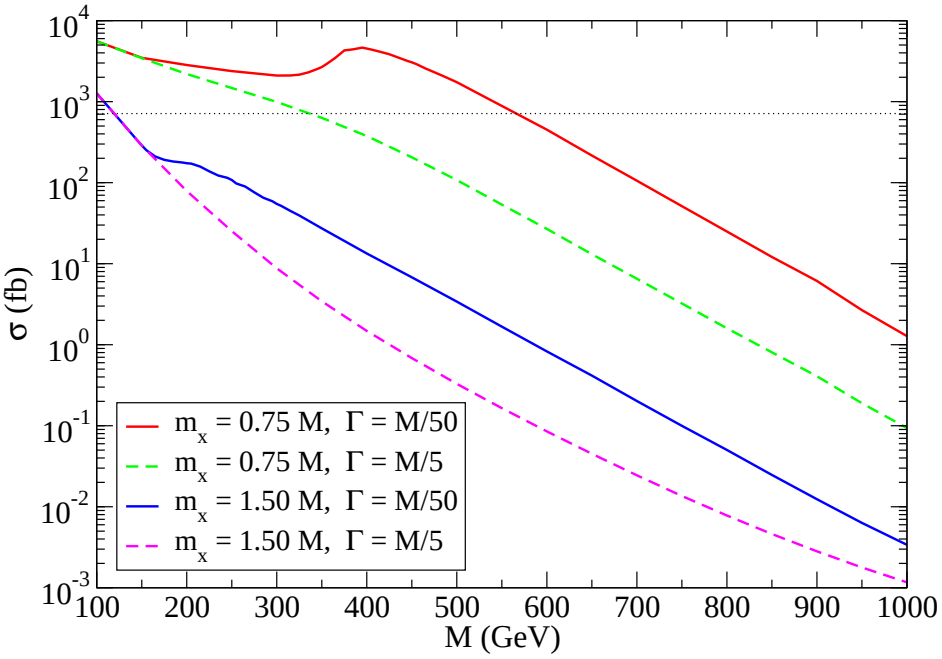

Figure 4: Leading-order monojet production cross sections at the Tevatron subject to the cuts described in the text. We show lines for $m_X = 0.7\,5M$, $1.50\,M$ and $\Gamma = M/5$, $M/50$, and we set $\lambda = 1$ and $\zeta = 0.7$. The horizontal dashed line represents the current Tevatron 2σ exclusion limit on the net monojet cross section as described in the text.

$\zeta = 0.7$. This figure shows a significant resonant enhancement when the intermediate state is narrow. A similar enhancement was seen in Ref. [32]. The resonant enhancement only becomes fully operational at $M \gtrsim 300$ GeV due to the cut on jet p_T. The horizontal dashed line in Fig. 4 represents the current Tevatron 2σ exclusion limit on the net monojet cross section of $664\,fb$ (after cuts) [30], based on the CDF analysis of Refs. [35, 36] which uses the same set of jet cuts as applied to our signal estimates. This limit translates into a lower bound of $M = 200-700$ GeV for the operator of Eq. (14), depending on the mass of the X state and the width of the unspecified intermediate state.

Monojet signals can also be detected at the LHC. Due to the expectation of a significant amount of associated QCD radiation, Ref. [37] investigated the reach of an inclusive search for a hard jet plus missing energy search at ATLAS with no veto on additional hard jets. To match this analysis, we compute the inclusive leading-order parton-level cross section at the LHC with $\sqrt{s} = 14$ TeV subject to the cuts $p_T > 500$ GeV and $|\eta| < 3.2$ on the outgoing jet. We also rescale the cross section by a conservative acceptance/efficiency factor of 85% [30]. The corresponding cross sections are shown in Fig. 5 for several values of M with $m_X = 0.75M$, $1.5M$ and $\Gamma = M/5$, $M/50$. We also set $\lambda = 1$ and $\zeta = 0.7$. Based on the background analysis of Ref. [37], the study in Ref. [30] estimated a net SM background production rate after the applied cuts of $\sigma_{BG} \simeq 200\,fb$. Applying a simple $S/\sqrt{B} > 5$ measure on the detection significance, this leads to a sensitivity to monojet cross sections as small as $70\,fb$ ($7\,fb$) with $1\,fb^{-1}$ ($100\,fb^{-1}$) of data at $\sqrt{s} = 14$ TeV. This is shown by

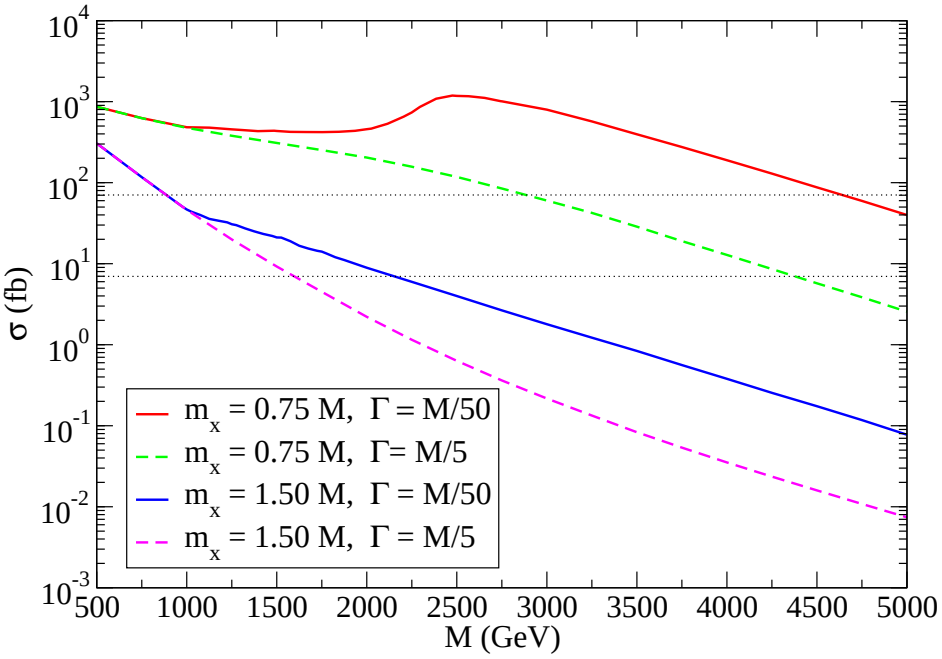

Figure 5: Jet plus missing energy production cross sections at the LHC (14 TeV) subject to the cuts described in the text. We show lines for $m_X = 0.75\,M$, $1.50\,M$ and $\Gamma = M/5$, $M/50$, and we set $\lambda = 1$ and $\zeta = 0.7$. The upper (lower) horizontal dotted line denotes the estimated discovery reach of the search described in the text with $1\,fb^{-1}$ ($100\,fb^{-1}$) of data.

the dotted lines in Fig. 5. The resulting LHC reach for the operator of Eq. (14) lies in the range $M = 1-4$ TeV. Recent inclusive LHC searches for jets plus missing energy using $1\,fb^{-1}$ of data at $\sqrt{s} = 7$ TeV and demanding a hard jet with $p_T > 120$ GeV and $|\eta| < 2.0$ bound cross sections (after cuts) up to $1.7\,pb$ [38, 39]. We find that this limits M to lie above $300-1900$ GeV depending on the specific values of m_X and Γ (chosen as above). These limits are competitive with the sensitivity to this operator from searches for IND in existing nucleon decay experiments.

Additional quark operators beyond that given in Eq. (14) and considered above are expected to yield qualitatively similar collider rates and signatures in most cases. An interesting further possibility are quark operators involving top or bottom quarks. With a bottom quark in the final state, the monojet signal could be augmented with a b-tag. In the case of a top quark in the final state, the signal would be a hard single top quark with large missing energy. While the search reach in monobottom and monotop channels is likely greater than for the light quark channels, the operators involving third-generation quarks do not correlate directly with IND processes.

The hylogenesis model in Ref. [15] also contains a hidden $U(1)'$ gauge symmetry that couples to (Ψ, Φ), is spontaneously broken at the GeV-scale, and couples to the SM only through kinetic mixing with hypercharge. Direct pair production of DM particles via the corresponding Z' vector boson with an associated jet can be another source of monojet

signals [30, 31]. However, since this vector is relatively light, the existing bounds from the Tevatron and the expected reach of the LHC are both much weaker than the limits from DM direct detection through elastic scattering mediated by the Z'.

4 IND and Stellar Evolution

DM can be captured in stars by elastic scattering with the nuclei they contain. Once captured, ordinary self-annihilating DM will collect in the middle of the star and annihilate with other DM particles there, releasing energy [40, 41, 42]. Self-annihilation is not possible for hylogenic dark matter (hDM) due to its conserved global charge. Instead, it can potentially destroy baryons within the star via IND processes such as $\Psi\, N \to \Phi^\dagger M$. If it remains within the star, the anti-hDM $\Phi^\dagger$ reaction product can then annihilate with a Φ particle already captured in the stellar core. The net result of this chain is the destruction of a baryon and the release of energy, both from the meson decay and the annihilation step.

In this section we investigate the effects of IND processes on several varieties of stellar species including neutron stars, white dwarfs, and main-sequence stars. To be concrete, we will concentrate on the specific model of hylogenesis presented in Ref. [15] and described in Appendix A with IND mediated by the operator of Eq. (1). We will assume a fiducial spin-independent proton scattering cross section of $\sigma_p^{SI} = 10^{-39}\,\mathrm{cm}^2$ (and $\sigma_n^{SI} = 0$) for both Ψ and Φ induced by their coupling to the kinetically-mixed $U(1)'$ vector boson,[5] as well as an hDM-anti-hDM annihilation cross section of $(\sigma v)_{ann} = 10^{-25}\mathrm{cm}^3/\mathrm{s}$. We shall consider two cases for the IND cross section: a large value of $(\sigma v)_{IND} = 10^{-39}\mathrm{cm}^3/\mathrm{s}$, and a small value of $(\sigma v)_{IND} = 0$. The general behaviour for other IND rates will lie somewhere between these two extremes.

4.1 Stellar Capture and Annihilation

Relic Ψ and Φ particles will be captured in stars by scattering with nuclei to energies below the local escape velocity. Once captured, an hDM particle will undergo further scatterings, thermalize with the baryons in the star, and collect within the stellar core. This occurs quickly relative to the lifetimes of the stars we consider here for our large fiducial value of the proton scattering cross section. Once they thermalize, the DM particles are largely confined to a core of radius [41, 42, 46]

$$r_{i,th} = \left(\frac{9T_c}{4\pi G \rho_c m_i}\right)^{1/2}, \tag{19}$$

where $i = \Psi, \Phi$, T_c is the mean temperature and ρ_c is the mean (baryon) density in the stellar core.

[5] For DM masses below 3 GeV, this value is consistent with existing direct detection searches [43, 44, 45].

The evolution of the total numbers of Ψ, Φ, $\bar{\Psi}$, and $\Phi^\dagger$ within a star is described the following system of equations:

$$\frac{dN_\Psi}{dt} = C_\Psi - A_\Psi N_\Psi N_{\bar{\Psi}} - B_\Psi N_\Psi \tag{20}$$

$$\frac{dN_{\bar{\Psi}}}{dt} = - A_\Psi N_\Psi N_{\bar{\Psi}} + \epsilon_{\bar{\Psi}} B_\Phi N_\Phi \tag{21}$$

$$\frac{dN_\Phi}{dt} = C_\Phi - A_\Phi N_\Phi N_{\Phi^\dagger} - B_\Phi N_\Phi \tag{22}$$

$$\frac{dN_{\Phi^\dagger}}{dt} = - A_\Phi N_\Phi N_{\Phi^\dagger} + \epsilon_{\Phi^\dagger} B_\Psi N_\Psi \tag{23}$$

Here, the C_i coefficients are the hDM capture rates, the A_i coefficients describe hDM-anti-hDM annihilation, and the B_i coefficients describe IND. A general expression for C_i is given in Ref. [42], while the A and B coefficients are given to a good approximation by

$$A_i \simeq (\sigma v)_{i,ann} \Big/ \left(4\pi r_{i,th}^3/3\right), \tag{24}$$

$$B_i \simeq (\sigma v)_{i,IND}\, (\rho_c/m_n), \tag{25}$$

where m_n is the mass of a nucleon. The ϵ_i terms appearing in Eqs. (21) and (23) are the probabilities for the anti-hDM products of IND to be captured by the host star after they are created. In certain regimes additional processes can influence the evolution of the stellar populations of hDM and anti-hDM such as evaporation [41, 47] and direct annihilation to baryons (*e.g.* $\Psi\,\Phi \to \bar{N}\,M$). We will discuss these effects when they may be relevant.

4.2 Neutron Stars

Neutron stars are very dense objects supported by the Fermi degeneracy pressure of their neutrons. Despite their name, they also contain a significant mass fraction of protons and heavier nuclei, and the nuclear state of their cores is not fully understood [48]. Typical neutron star parameters are mass $M = 1.4 M_\odot$, with $M_\odot \simeq 2.0 \times 10^{30}$ kg the solar mass, radius $R = 10\,\mathrm{km}$, core temperature $T_c = 10^5\,\mathrm{K}$, and core baryon density $\rho_c = 1.4 \times 10^{18} \mathrm{kg\,/m^3}$ [46, 49, 50, 51].

The rate of capture of Ψ or Φ upon a typical neutron star (including general relativistic corrections) is [49, 50, 51]

$$C_i \simeq 2.5 \times 10^{25} \mathrm{s}^{-1} \left(\frac{\rho_{DM}}{\mathrm{GeV/cm^3}}\right) \left(\frac{5\ \mathrm{GeV}}{m_\Psi + m_\Phi}\right) \left(\frac{220\,\mathrm{km/s}}{\bar{v}}\right) f, \tag{26}$$

where ρ_{DM} is the local DM energy density, $\bar{v}$ is the local DM velocity dispersion, and

$$f = min\left\{1,\, (x_p \sigma_p + x_n \sigma_n)/(2 \times 10^{-45}\,\mathrm{cm}^2)\right\}, \tag{27}$$

with x_p and x_n being the proton and neutron mass fractions. The factor f accounts for the saturation of the cross section at the cross-sectional area of the star. This saturation sets

in when the star becomes optically thick to DM – when a DM particle impinging upon the star is likely to scatter multiple times with nucleons in the star. For the fiducial nucleon scattering cross section we are using and assuming a proton mass fraction of $x_p = 0.1$, we find that neutron stars are optically thick to both Ψ and Φ. This leads to $C_\Psi = C_\Phi \equiv C$ as well as $\epsilon_\Psi = 1 = \epsilon_\Phi$. We also find

$$r_{i,th} \simeq (140\,\mathrm{cm}) \left(\frac{T_c}{10^5\,\mathrm{K}}\right)^{1/2} \left(\frac{3\,\mathrm{GeV}}{m_i}\right)^{1/2} \left(\frac{1.4\times 10^{18}\mathrm{kg/m^3}}{\rho_c}\right)^{1/2}, \tag{28}$$

implying $A_i \sim 5\times 10^{-32}\mathrm{s}^{-1}$ and $B_i \sim 0.9\,\mathrm{s}^{-1}$ ($0\,\mathrm{s}^{-1}$) for the large (small) IND rate $(\sigma v)_{IND} = 10^{-39}\mathrm{cm}^3/\mathrm{s}$ ($0\,\mathrm{cm}^3/\mathrm{s}$).

Consider first the case of a large IND rate. Using the evolution equations of Eqs. (20–23) and assuming negligible initial hDM densities, we find that the numbers of hDM and anti-hDM particles within a typical neutron star reach a steady state. This behaviour is shown in Fig. 6 for the fiducial cross sections given above and $m_\Psi = 2.85$ GeV, $m_\Phi = 2.05$ GeV. The steady-state populations in the limit of $B_i \gg A_i$ are approximated well by the analytic expressions

$$N_\Psi \simeq \frac{C}{B_\Psi(1+\xi)},\ N_{\bar\Psi} \simeq \frac{B_\Psi}{A_\Psi}\left(\frac{1+\xi}{1+\xi^{-1}}\right),\ N_\Phi \simeq \frac{C}{B_\Phi(1+\xi^{-1})},\ N_{\Phi^\dagger} \simeq \frac{B_\Phi}{A_\Phi}\left(\frac{1+\xi^{-1}}{1+\xi}\right), \tag{29}$$

with $\xi = A_\Psi B_\Phi / A_\Phi B_\Psi$.[6] A steady state is also attained when one of the IND rates vanishes due to kinematic suppression. For example, with $B_\Psi \gg A_{\Psi,\Phi}$ and $B_\Phi \to 0$, we find

$$N_\Psi = \frac{C}{B_\Psi}, \quad N_{\bar\Psi} = 0, \quad N_{\Phi,\Phi^\dagger} = \pm\frac{C}{2B_\Psi} + \sqrt{\left(\frac{C}{2B_\Psi}\right)^2 + \frac{C}{A_\Phi}}, \tag{30}$$

where in the last equality the plus sign corresponds to Φ and the minus sign to $\Phi^\dagger$. The solution for $B_\Psi \to 0$ and $B_\Phi \gg A_{\Psi,\Phi}$ is identical but with Φ and Ψ interchanged in the expressions above. In both cases, the steady-state particle populations are on the order of $N_{\Psi,\Phi} \simeq 10^{25}$ and $N_{\bar\Psi,\Phi^\dagger} \simeq 10^{31}$ (when they are non-zero) for the fiducial input values listed above.

The time needed to reach this steady state from a negligible initial dark matter density in the star is on the order of

$$\tau_{ss} \sim max\left\{B^{-1}, \frac{B}{CA}\right\}. \tag{31}$$

where the first value corresponds to IND balancing capture and the second to annihilation balancing production of anti-hDM by IND. For the fiducial cross sections we are considering, we find that annihilation takes longer to balance, and leads to $\tau_{ss} \sim 2\times 10^7\,\mathrm{s}$. This is ultra short relative to the lifetime of a typical neutron star.

Having reached a steady state, the main combined effect of the IND and annihilation processes is to inject energy into the host neutron star with rate $(m_\Psi + m_\Phi + m_N)C$. In

[6] For $A_i \gg B_i$, we find: $N_\Psi = N_\Phi = C/(B_\Psi + B_\Phi),\ N_{\bar\Psi} = B_\Phi/A_\Psi,\ N_{\Phi^\dagger} = B_\Psi/A_\Phi$.

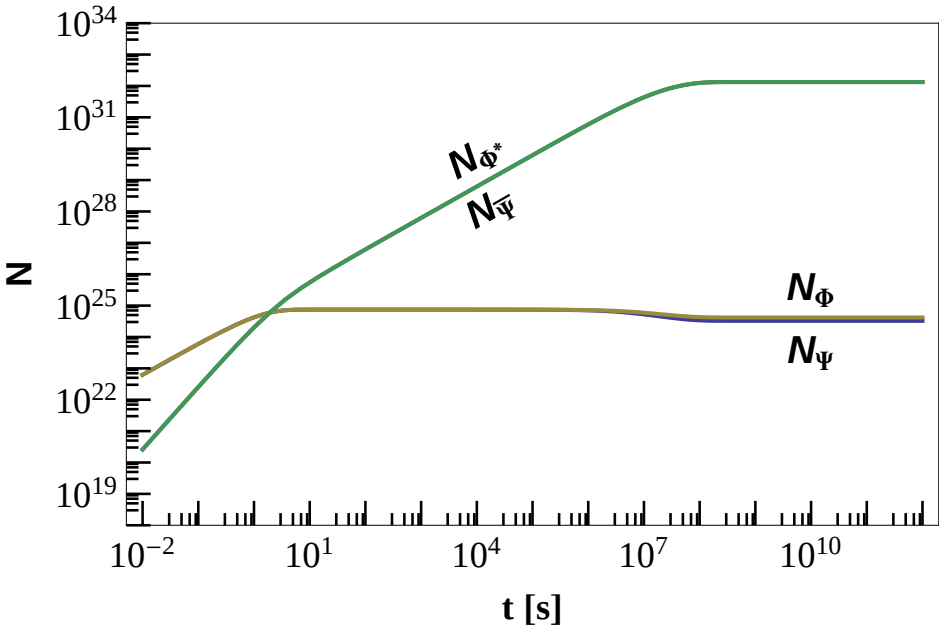

Figure 6: The build-up of the abundance of hDM and anti-hDM in a neutron star for $m_\Psi = 2.85$ GeV and $m_\Phi = 2.05$ GeV for a total dark matter density of 0.3 GeV/cm^3. At this density a steady state is attained after a little over 10^7 s.

this respect, hDM in the steady state limit has the same effect on neutron stars as ordinary self-annihilating DM. Energy injection by DM can interfere with and halt the cooling of old neutron stars, and therefore the observation of a very cool, old neutron star in a region of large DM density could put significant constraints on a wide variety of DM scenarios [46, 50, 51]. However, this effect is too small to be observed using existing observations, and appears to be challenging to probe in the near future [46, 50, 51]. With hDM, baryons within the neutron star are also destroyed by IND, but the number is negligible compared to the total of $N_B \simeq 2 \times 10^{57}$ within a typical neutron star over the lifetime of the Universe unless the local DM density approaches an enormous value of $10^{14}\,\mathrm{GeV/cm^3}$.

Consider next the case of a vanishingly small IND cross section. The populations of of Ψ and Φ hDM particles will now build up within the neutron star with rate given by Eq. (26), corresponding to populations of about $10^{43}(\rho_{DM}/\,\mathrm{GeV\,cm^{-3}})$ over the lifetime of the Universe. We can compare this number to the populations required for DM particles to begin self-gravitating and to form a black hole. Self-gravitation begins when [46, 52, 53]

$$N_i \gtrsim N_{self} \equiv \frac{\rho_c}{m_i}(4\pi r_{i,th}^3/3) \simeq 3 \times 10^{45} \left(\frac{3\,\mathrm{GeV}}{m_i}\right)^{5/2} \left(\frac{T_c}{10^5\mathrm{K}}\right)^{3/2} \left(\frac{1.4 \times 10^{18}\mathrm{kg/m^3}}{\rho_c}\right)^{1/2}. \quad (32)$$

This is much greater than the steady-state populations found above for the case of a large IND rate, and also greater than the numbers collected for a smaller IND rates for local hDM densities below $(3 \times 10^2\,\mathrm{GeV/cm^3})\,min\{1,\ 3 \times 10^{-57}\mathrm{cm^3 s^{-1}}/(\sigma v)_{IND}\}$.

Self-gravitating DM particles will form a black hole that can potentially destroy the host

star unless they are stabilized in some way [46, 49, 52, 53, 54]. For non-interacting fermions there is a degeneracy pressure that must be overcome. To do so, the total number of fermions must exceed

$$N_i \gtrsim N_{crit}^f \equiv \left(\frac{\sqrt{8\pi} M_{\rm Pl}}{m_i}\right)^3 \simeq 6 \times 10^{55} \left(\frac{3 \text{ GeV}}{m_i}\right)^3, \tag{33}$$

with $M_{\rm Pl} = \sqrt{8\pi/G} \simeq 2.4 \times 10^{18}\,\text{GeV}$ the reduced Planck mass. In the case of non-self-interacting bosons, there is still a zero-point pressure which can be overcome if the number of bosons exceeds

$$N_i \gtrsim N_{crit}^b \equiv \left(\frac{\sqrt{8\pi} M_{\rm Pl}}{m_i}\right)^2 \simeq 2 \times 10^{37} \left(\frac{3 \text{ GeV}}{m_i}\right)^2. \tag{34}$$

A bosonic black hole can also arise even before bulk self-gravitation sets in through the formation of a Bose-Einstein condensate [52, 53].

We argue that black holes are not likely to form in the specific theory of hylogenesis discussed in Ref. [15] and Appendix A, in which Φ and Ψ carry equal and opposite charges under a spontaneously broken $U(1)'$ gauge symmetry, until $N_{\Psi,\Phi} > N_{crit}^f$. At distances much smaller than the inverse vector mass $m_{Z'}^{-1}$, the effects of breaking the $U(1)'$ can be neglected and the Z' vector boson mediates a repulsive force between particles with like-sign charges. This induces a pressure among Φ particles that prevents them from collapsing into a black hole provided $m_{Z'} \ll (m_\Phi M_{\rm Pl}^2)^{1/3}$ and $e' \gg m_\Phi/M_{\rm Pl}$ (where e' is the $U(1)'$ coupling of Φ) [52]. Instead, under these mild assumptions the formation of a black hole requires an approximately charge-neutral collection of hDM particles and therefore roughly equal numbers of Ψ and Φ states. A necessary condition for this to occur is $N > N_{crit}^f$ to overcome the fermion degeneracy pressure. Therefore we do not expect this specific theory of hylogenesis to lead to the formation of hDM black holes within neutron stars unless the local hDM density around the host star exceeds 5×10^{11} GeV/cm^3.

Between the two extremes of the large and small IND rates considered above, no new obvious observational bounds arise. With a small but non-zero rate for IND, the Ψ and Φ populations may grow large enough to form some amount of anti-hDM that will subsequently annihilate away. Large hDM densities can also lead to direct annihilation of hDM to antibaryons, $\Psi\,\Phi \to \bar{N}\,M$, and similarly for anti-hDM. This can be accounted for by adding terms of the form $-D N_\Psi N_\Phi$ to the evolution equations for Ψ and Φ, with $D \simeq (\sigma v)_{IND}/V_{hDM}$ and V_{hDM} is the volume occupied by the hDM, whose evolution we must also keep track of. Note that V_{hDM} appears here rather than $4\pi r_{th}^3/3$ because this effect starts to compete with standard IND only after the hDM population begins to self-gravitate, when $N_i > \rho_c V_{hDM}/V > N_{self}$. We defer an analysis of the effects of self-gravitation and self-annihilation of hDM on the structure of neutron stars to a future work.

4.3 White Dwarfs

We can perform a similar analysis for the effects of hDM on white dwarfs. A typical white dwarf consists primarily of carbon and oxygen and is supported by the degeneracy pressure

of the electrons it contains. Typical white dwarf parameters are $R = 0.01\,R_\odot$, $M = 0.7\,M_\odot$, $\rho_c = 10^9\,\mathrm{kg/m}^3$, $T_c = 10^7\,\mathrm{K}$ [55]. We will approximate the internal structure of a white dwarf as consisting entirely of carbon with a uniform density [46].

The capture rate of DM through elastic scattering with nuclei in a white dwarf is approximated well by the expression [42, 46, 56, 57, 58]

$$C_i \simeq \left(\frac{8}{3\pi}\right)^{1/2}\left(\frac{\rho_i \bar{v}}{m_i}\right)\left(\frac{3v_{esc}^2}{2\bar{v}^2}\right)\sigma_{eff}, \tag{35}$$

with $\bar{v}$ being the local velocity dispersion, v_{esc} the escape velocity at the surface of the star, and the the effective cross section is defined to be

$$\sigma_{eff} \equiv min\left\{\pi R^2,\ \ \sigma_p^{SI}\sum_k \frac{M}{m_n}\frac{x_k}{A_k}\frac{[f_p Z_k + (A_k - Z_k)f_n]^2}{f_p^2}\left(\frac{m_{r_k}}{m_{r_p}}\right)^2\right\}, \tag{36}$$

where the sum runs over all nuclear species k in the star with mass fraction x_k and atomic mass (number) A_k (Z_k), σ_p^{SI} is the spin-independent nucleon scattering cross section off protons, f_p and f_n are the relative coupling strengths of the DM to protons and neutrons, and m_{r_k} (m_{r_p}) is the reduced mass of the DM-nucleus (DM-proton) system. The saturation of the effective cross section at πR^2 corresponds to the star becoming optically thick.

We find that a typical white dwarf is indeed optically thick for the fiducial scattering cross section of $\sigma_p^{SI} = 10^{-39}\mathrm{cm}^2$ (with $f_p = 1$, $f_n = 0$). This gives

$$\begin{aligned} C_\Psi &= C_\Phi \equiv C \\ &\simeq (6\times 10^{27}\mathrm{s}^{-1})\left(\frac{R}{0.01R_\odot}\right)\left(\frac{M}{0.7M_\odot}\right)\left(\frac{\rho_{hDM}}{\mathrm{GeV/cm}^3}\right)\left(\frac{5\ \mathrm{GeV}}{m_\Psi + m_\Phi}\right)\left(\frac{270\,\mathrm{km/s}}{\bar{v}}\right), \end{aligned} \tag{37}$$

where $R_\odot \simeq 7.0\times 10^5$ km is the solar radius. Once captured, hDM particles thermalize rapidly and collect within a thermal radius at the core of the star of size

$$r_{i,th} \simeq (5\times 10^7\,\mathrm{cm})\left(\frac{3\ \mathrm{GeV}}{m_i}\right)^{1/2}\left(\frac{T_c}{10^7\mathrm{K}}\right)^{1/2}\left(\frac{10^9\mathrm{kg/m}^3}{\rho_c}\right)^{1/2}. \tag{38}$$

For $m_\Psi = m_\Phi = 2.25$ GeV, we find $A_i = 1\times 10^{-49}\mathrm{s}^{-1}$ and $B_i = 6\times 10^{-10}\mathrm{s}^{-1}$ ($0\,\mathrm{s}^{-1}$) for the case of a large (small) IND rate $(\sigma v)_{IND} = 10^{-39}\mathrm{cm}^3/\mathrm{s}$ ($0\,\mathrm{cm}^3/\mathrm{s}$)

In the case of a large IND rate, we find that the populations of Ψ, Φ, $\bar{\Psi}$, and $\Phi^\dagger$ all reach a steady state quickly relative to the lifetime of a typical white dwarf. In this state we find $N_\Psi \simeq N_\Phi \simeq 5\times 10^{36}$ and $N_{\bar{\Psi}} \simeq N_{\Phi^\dagger} \simeq 6\times 10^{49}$ for the fiducial parameter values listed above. The number of baryons destroyed by IND over the age of the Universe is a small fraction of the total number in a white dwarf provided $\rho_{DM} \ll 10^{11}$ GeV/cm^3. The main effect of hDM capture, IND, and annihilation on white dwarf is therefore the injection of energy into the stellar interior with rate $(m_\Psi + m_\Phi + m_N)C$. This is equivalent to the effect of ordinary self-annihilating DM (with slightly larger mass).

Heating of white dwarfs by DM capture and annihilation was studied recently in Refs. [46, 57, 58]. These authors differ in their conclusions, with Ref. [57] finding an upper bound on

the nuclear capture cross section of about 10^{-43}cm^2 and Ref. [58] finding essentially no bounds from current observations. The origin of the disagreement is the density of DM within globular clusters, from which Ref. [57] obtains their most stringent bounds, while Ref. [58] argues that they contain a much smaller dark matter abundance. The observation of a cool white dwarf within a dwarf spheroidal galaxy could help to resolve this question decisively [58]. Based on this uncertainty, we do not consider hDM models with nuclear scattering cross sections as large as $\sigma_p^{SI} = 10^{-39}\text{cm}^2$ to be ruled out. However, we do note that the model of hDM considered here can also accommodate much smaller elastic scattering cross sections.

With a small IND rate, hDM collects and builds up within the stellar interior. As we argued above, we do not expect any significant effects on the star until at least $N_i \sim N_{self}$, N_{crit}^f given in Eqs. (32,33). For this to occur over the lifetime of the Universe, a local hDM density approaching $10^8 - 10^{10}\,\text{GeV/cm}^3$ is needed. We do not know of any observations of white dwarfs that approach these requirements.

4.4 The Sun and other Main-Sequence Stars

The capture rate of light (1–5 GeV) DM in the sun is dominated by scattering with hydrogen and helium and is given to a good approximation by [42, 59]

$$C_i \simeq (8\times 10^{25}\text{s}^{-1})\left(\frac{5\,\text{GeV}}{m_\Psi + m_\Phi}\right)\left(\frac{\rho_{DM}}{0.3\,\text{GeV/cm}^3}\right)\left(\frac{270\,\text{km/s}}{\bar{v}}\right)\left(\frac{\sigma_p^{SI}}{10^{-39}\text{cm}^2}\right) \times\left[x_H + (1.1)x_{He}(1+f_n/f_p)^2\frac{m_{r_{He}}^2}{m_{r_p}^2}\right], \tag{39}$$

where the relative factor for helium relative to hydrogen comes from its slightly different distribution within the sun. In writing this expression we have also made use of the fact that the sun is optically thin for our fiducial nucleon elastic scattering cross section. A second consequence of the sun being optically thin is that nearly all the anti-hDM produced by IND escapes from the sun, since it is typically produced with velocities much larger than v_{esc}. Thus we set $\epsilon_{\bar{\Psi},\Phi^\dagger} \to 0$ in our evolution equations. The thermal radius in which the DM collects is

$$r_{i,th} \simeq (5\times 10^9\,\text{cm})\left(\frac{3\text{ GeV}}{m_i}\right)^{1/2}\left(\frac{T_c}{1.5\times 10^7\text{K}}\right)^{1/2}\left(\frac{1.5\times 10^5\text{kg/m}^3}{\rho_c}\right)^{1/2} \tag{40}$$

which yields $B_i \sim 10^{-13}\,\text{s}^{-1}\,(0\,\text{s}^{-1})$ for the large (small) IND rate.

An additional effect that is important for the sun is evaporation, in which captured hDM particles are up-scattered above the escape velocity and leave the sun [41, 47]. Fitting to the results of Refs. [47, 59], we take the evaporation rate to be

$$E_i \simeq 10^{[-3.5(m_i/\,\text{GeV})-4]}\left(\frac{\sigma_p^{SI}}{5\times 10^{-39}\text{cm}^2}\right)\text{s}^{-1}. \tag{41}$$

This evaporation adds a dissipative $-E_i N_i$ term to each of Eqs. (20–23). For the fiducial parameters we are considering (and a large IND rate), evaporation becomes more important than IND for hDM masses below $m_i \lesssim 2.4$ GeV.

We find that capture, evaporation, and IND reach a steady state on a timescale of 10^{-5}-10^{-1} billion years, much shorter than the age of the sun. The equilibrium populations are always less than $N_i \simeq C_i/max\{B_i, E_i\} \lesssim 10^{41}$, for both large and small IND rates. This is a very small fraction of the total mass of the sun, and is far below what is needed for hDM to self-gravitate or to contribute significantly to the properties of the solar interior [60]. Note as well that due to the low masses of hDM, the energies of any neutrinos produced by IND are well below the thresholds of DM searches for upward-going muons in neutrino telescopes such as Ice Cube [59, 61]. The effects of hDM on other main-sequence stars are also expected to be small, unless the star is immersed in a region of very large DM density [62].

5 Conclusions

We have investigated signals of nucleon destruction that can arise in specific theories where dark matter is antibaryonic. Antibaryonic DM is motivated by unified mechanisms for DM and baryon generation (referred to as hylogenesis) which address the cosmic coincidence between the energy densities of dark and visible matter in the Universe.

In the hylogenesis scenario considered here, the DM consists of an asymmetric density of fermions Ψ and scalars Φ. These particles can scatter inelastically with nucleons via the reactions $\Psi N \to \Phi^\dagger M$ and $\Phi N \to \bar{\Psi} M$, where N is a nucleon and M is a meson. These induced nucleon decay (IND) processes lead to distinctive signatures in nucleon decay searches, stellar evolution, and hadron colliders.

IND is a novel signature of DM that can be searched for in terrestrial nucleon decay searches. The effective nucleon lifetime is expected to be $\sim 10^{29} - 10^{32}$ years, if baryon transfer between dark and visible sectors is mediated by new physics at a scale $\Lambda \sim 300\,\mathrm{GeV} - 1\,\mathrm{TeV}$. Since the DM states are unobserved, IND events mimic standard nucleon decay with neutrino final states, but typically with greater final state meson energy $E \sim$ GeV. Due to these different kinematics, existing searches do not directly apply in general. Our study therefore motivates new searches in these experiments. We expect that the resulting sensitivities should be comparable to those in standard nucleon decay searches.

The coupling of hylogenic DM to quarks responsible for IND can also give rise to observable signals in hadron colliders. In particular, such couplings can potentially lead to monojet signals at the Tevatron and the LHC. Existing monojet searches at the Tevatron place a lower bound on the coupling of hylogenic DM to quarks, and this bound will be significantly improved at the LHC. We find that the coupling strengths that can be probed at the LHC are of the same size as those that can produce an observable effect in nucleon decay search experiments. This correlation may permit the characterization of hylogenic DM through a very diverse set of experimental probes.

If hylogenic DM also scatters elastically with nucleons, it can be captured in stars. Once

captured, it will thermalize with the baryons in the star and sink to the stellar core. In compact stars, the local baryon density in the stellar core may be large enough for IND to occur at a significant rate, destroying both a nuclon and the hDM particle, and producing an anti-hDM particle and a meson. This process deposits energy in the star, an effect that may be probed by observing old and cool neutron stars or white dwarfs. However, current observations do not provide a definitive bound on or evidence for these processes.

Acknowledgements

We thank Brian Batell, Matthew Buckley, Robert Caldwell, Alejandra Castro, Jim Cline, Katie Freese, Patrick Fox, Michael Graesser, Ed Kearns, Jennifer Kile, John Ng, Scott Oser, Maxim Pospelov, Michael-Ramsey-Musolf, Jen Raaf, Adam Ritz, Pat Scott, Rishi Sharma, Hirohisa Tanaka, and Kathryn Zurek for helpful discussions. We also thank Jennifer Kile for collaboration in the early stages of this work. DM and ST would like to thank the Weizmann Institute of Science for their hospitality. KS would like to thank Perimeter Institute for Theoretical Physics for their hospitality. The work of HD is supported by the United States Department of Energy under Grant Contract DE-AC02-98CH10886. The work of DM, KS, and ST is supported by the National Science and Engineering Research Council of Canada (NSERC).

A Appendix

In this Appendix we review some of the important features of the hylogenesis model presented in Ref. [15]. The model consists of the SM together with a SM-neutral hidden sector containing two massive Dirac fermions X_a ($a = 1, 2$, with masses $m_{X_2} > m_{X_1} \gtrsim$ TeV), a Dirac fermion Ψ, and a complex scalar Φ (with masses $m_\Psi \sim m_\Phi \sim$ GeV). These fields couple through the "neutron portal" ($XU^cD^cD^c$) and a Yukawa interaction:

$$-\mathscr{L} \supset \frac{\lambda_a^{ijk}}{M^2}\,(X_{a,L}^\dagger d_R^k)(u_R^i d_R^j) + \zeta_a\,(X_{a,L}\Psi_L + X_{a,R}\Psi_R)\Phi + \text{h.c.} \tag{42}$$

where i, j, k label flavors and the quark color indices are implicitly contracted antisymmetrically. Many variations on these operators exist, corresponding to different combinations of quark flavors and spinor contractions. With this set of interactions one can define a conserved generalized global baryon number with charges $B_X = -(B_\Psi + B_\Phi) = 1$. The proton, Ψ, and Φ are stable due to their B and gauge charges if their masses satisfy

$$|m_\Psi - m_\Phi| < m_p + m_e, \qquad m_p - m_e < m_\Psi + m_\Phi\ . \tag{43}$$

Ψ and Φ are the "hidden antibaryons" that comprise the dark matter. Furthermore, there exists a physical CP-violating phase $\arg(\lambda_1^*\lambda_2\zeta_1\zeta_2^*)$ that cannot be removed through phase redefinitions of the fields.

We also introduce a hidden $U(1)'$ gauge symmetry under which Ψ and Φ have opposite charges $\pm e'$, while X_a is neutral. We assume this symmetry is spontaneously broken at the GeV scale, and has a kinetic mixing with SM hypercharge $U(1)_Y$ via the coupling $-\frac{\kappa}{2}B_{\mu\nu}Z'_{\mu\nu}$, where $B_{\mu\nu}$ and $Z'_{\mu\nu}$ are the $U(1)_Y$ and $U(1)'$ field strength tensors. At energies well below the electroweak scale the effect of this mixing is primarily to generate a vector coupling of the massive Z' gauge boson to SM particles with strength $-c_W \kappa\, Q_{em} e$. The GeV-scale Z' masses we consider here can be consistent with observations for $10^{-6} \lesssim \kappa \lesssim 10^{-2}$ [63, 64].

In the mechanism for hylogenesis presented in Ref. [15], baryogenesis begins when a non-thermal, CP-symmetric population of X_1 and $\bar{X}_1$ is produced in the early Universe. These states decay through $X_1 \to udd$ or $X_1 \to \bar{\Psi}\Phi^\dagger$ (and their conjugates). An asymmetry between the partial widths for $X_1 \to udd$ and $\bar{X}_1 \to \bar{u}\bar{d}\bar{d}$ arises from interference between tree and loop diagrams and is characterized by

$$\epsilon = \frac{1}{2\Gamma_{X_1}}\left[\Gamma(X_1 \to udd) - \Gamma(\bar{X}_1 \to \bar{u}\bar{d}\bar{d})\right] \simeq \frac{m_{X_1}^5 \,\mathrm{Im}[\lambda_1^* \lambda_2 \zeta_1 \zeta_2^*]}{256\pi^3 \,|\zeta_1|^2 \, M^4 m_{X_2}}\,, \tag{44}$$

where we have assumed that the total decay rate Γ_{X_1} is dominated by $X_1 \to \bar{\Psi}\Phi^\dagger$ over the three-quark mode, and that $m_{X_2} \gg m_{X_1}$. For $\epsilon \neq 0$, X_1 decays generate a baryon asymmetry in the visible sector, and by CPT an equal and opposite baryon asymmetry in the hidden sector. These asymmetries can be "frozen in" by the weakness of the coupling between both sectors provided the temperature at which the X_1 are produced is not too high. For the asymmetry to be large enough to explain the observed value, $m_{X_{1,2}}$ cannot be too much smaller than M.

Once produced, Ψ and Φ will thermalize by scattering with Z' vectors present in the plasma. These interactions will also deplete the symmetric densities of Ψ and Φ very efficiently through annihilation to pairs of Z' vectors provided $m_{Z'} < m_{\Psi,\Phi}$ [65]. Only the asymmetries will remain. This is analogous to the annihilation of baryons with antibaryons. The cross section for $\Psi\bar{\Psi} \to Z'Z'$ is given by [66]

$$\langle \sigma v \rangle = \frac{e'^4}{16\pi}\frac{1}{m_\Psi^2}\sqrt{1 - m_{Z'}^2/m_\Psi^2} \simeq (1.6 \times 10^{-25}\mathrm{cm}^3/\mathrm{s})\left(\frac{e'}{0.05}\right)^4\left(\frac{3\ \mathrm{GeV}}{m_\Psi}\right)^2. \tag{45}$$

Annihilation of $\Phi^\dagger\Phi$ is given by a similar expression.

There is also a direct detection signal in our model due to the hidden Z' mediating the elastic scattering of Ψ and Φ off protons. The effective scattering cross section per nucleon for either Ψ or Φ is spin-independent and given by

$$\sigma_0^{SI} = (5 \times 10^{-39}\mathrm{cm}^2)\left(\frac{2Z}{A}\right)^2\left(\frac{\mu_N}{\mathrm{GeV}}\right)^2\left(\frac{e'}{0.05}\right)^2\left(\frac{\kappa}{10^{-5}}\right)^2\left(\frac{0.1\,\mathrm{GeV}}{m_{Z'}}\right)^4, \tag{46}$$

where μ_N is the DM-nucleon reduced mass. For a DM mass of 2.9 GeV, this is slightly below the best current limits from CRESST [43], CDMS [44], and CoGeNT [45].

References

[1] E. Komatsu *et al.* [WMAP Collaboration], Astrophys. J. Suppl. **192**, 18 (2011). [1001.4538 [astro-ph.CO]].

[2] For reviews, see: A. Riotto, M. Trodden, Ann. Rev. Nucl. Part. Sci. **49**, 35-75 (1999). [hep-ph/9901362]; M. Dine, A. Kusenko, Rev. Mod. Phys. **76**, 1 (2004). [hep-ph/0303065]; S. Davidson, E. Nardi, Y. Nir, Phys. Rept. **466**, 105-177 (2008). [0802.2962 [hep-ph]].

[3] For reviews, see:
G. Jungman, M. Kamionkowski, K. Griest, Phys. Rept. **267**, 195-373 (1996). [hep-ph/9506380]; G. Bertone, D. Hooper, J. Silk, Phys. Rept. **405**, 279-390 (2005). [hep-ph/0404175].

[4] S. Nussinov, Phys. Lett. **B165**, 55 (1985); S. M. Barr, R. S. Chivukula, E. Farhi, Phys. Lett. **B241**, 387-391 (1990). S. M. Barr, Phys. Rev. **D44**, 3062-3066 (1991); D. B. Kaplan, Phys. Rev. Lett. **68**, 741-743 (1992); D. E. Kaplan, M. A. Luty, K. M. Zurek, Phys. Rev. **D79**, 115016 (2009). [0901.4117 [hep-ph]]; G. D. Kribs, T. S. Roy, J. Terning, K. M. Zurek, Phys. Rev. **D81**, 095001 (2010). [0909.2034 [hep-ph]]; T. Cohen, D. J. Phalen, A. Pierce, K. M. Zurek, Phys. Rev. **D82**, 056001 (2010), [1005.1655 [hep-ph]].

[5] D. Hooper, J. March-Russell, S. M. West, Phys. Lett. **B605**, 228-236 (2005). [hep-ph/0410114].

[6] R. Kitano, I. Low, Phys. Rev. **D71**, 023510 (2005). [hep-ph/0411133]; R. Kitano, I. Low, [hep-ph/0503112].

[7] K. Agashe, G. Servant, JCAP **0502**, 002 (2005). [hep-ph/0411254].

[8] G. R. Farrar, G. Zaharijas, Phys. Rev. Lett. **96**, 041302 (2006). [hep-ph/0510079].

[9] J. Shelton, K. M. Zurek, Phys. Rev. **D82**, 123512 (2010). [1008.1997 [hep-ph]]; N. Haba, S. Matsumoto, [1008.2487 [hep-ph]]; M. R. Buckley, L. Randall, [1009.0270 [hep-ph]]; E. J. Chun, Phys. Rev. **D83**, 053004 (2011). [1009.0983 [hep-ph]]; J. McDonald, [1009.3227 [hep-ph]]; M. Blennow, B. Dasgupta, E. Fernandez-Martinez, N. Rius, JHEP **1103**, 014 (2011), [1009.3159 [hep-ph]]; L. J. Hall, J. March-Russell, S. M. West, [1010.0245 [hep-ph]]; B. Dutta, J. Kumar, Phys. Lett. **B699**, 364-367 (2011). [1012.1341 [hep-ph]]; A. Falkowski, J. T. Ruderman, T. Volansky, JHEP **1105**, 106 (2011), [1101.4936 [hep-ph]]; E. J. Chun, JHEP **1103**, 098 (2011), [1102.3455 [hep-ph]]; Z. Kang, J. Li, T. Li, T. Liu, J. Yang, [1102.5644 [hep-ph]]; J. J. Heckman, S. -J. Rey, [1102.5346 [hep-th]]; D. E. Kaplan, G. Z. Krnjaic, K. R. Rehermann, C. M. Wells, [1105.2073 [hep-ph]]. M. T. Frandsen, S. Sarkar, K. Schmidt-Hoberg, [1103.4350 [hep-ph]]; A. Hook, [1105.3728 [hep-ph]]; N. F. Bell, K. Petraki, I. M. Shoemaker, R. R. Volkas, [1105.3730 [hep-ph]]; C. Cheung, K. M. Zurek, [1105.4612 [hep-ph]].

[10] P. Hut, K. A. Olive, Phys. Lett. **B87**, 144-146 (1979).

[11] S. Dodelson, L. M. Widrow, Phys. Rev. **D42**, 326-342 (1990).

[12] V. A. Kuzmin, Phys. Part. Nucl. **29**, 257-265 (1998). [hep-ph/9701269].

[13] P. -H. Gu, Phys. Lett. **B657**, 103-106 (2007). [0706.1946 [hep-ph]]; P. -H. Gu, U. Sarkar, X. Zhang, Phys. Rev. **D80**, 076003 (2009). [0906.3103 [hep-ph]]; P. -H. Gu, M. Lindner, U. Sarkar, X. Zhang, [1009.2690 [hep-ph]].

[14] H. An, S. -L. Chen, R. N. Mohapatra, Y. Zhang, JHEP **1003**, 124 (2010). [0911.4463 [hep-ph]]; H. An, S. -L. Chen, R. N. Mohapatra, S. Nussinov, Y. Zhang, Phys. Rev. **D82**, 023533 (2010). [1004.3296 [hep-ph]].

[15] H. Davoudiasl, D. E. Morrissey, K. Sigurdson, S. Tulin, Phys. Rev. Lett. **105**, 211304 (2010). [1008.2399 [hep-ph]].

[16] D. J. H. Chung, B. Garbrecht, S. Tulin, JCAP **0903**, 008 (2009). [0807.2283 [hep-ph]].

[17] S. Dimopoulos, L. J. Hall, Phys. Lett. **B196**, 135 (1987); J. M. Cline, S. Raby, Phys. Rev. **D43**, 1781-1787 (1991); S. D. Thomas, Phys. Lett. **B356**, 256-263 (1995). [hep-ph/9506274]; R. Kitano, H. Murayama, M. Ratz, Phys. Lett. **B669**, 145-149 (2008). [0807.4313 [hep-ph]]; R. Allahverdi, B. Dutta, K. Sinha, Phys. Rev. **D83**, 083502 (2011). [1011.1286 [hep-ph]].

[18] K. Kobayashi *et al.* [Super-Kamiokande Collaboration], Phys. Rev. **D72**, 052007 (2005). [hep-ex/0502026].

[19] For a review of various aspects of nucleon stability within unified models, see, for example, P. Nath, P. Fileviez Perez, Phys. Rept. **441**, 191-317 (2007). [hep-ph/0601023].

[20] D. Wall *et al.* [Soudan 2 Collaboration], Phys. Rev. **D62**, 092003 (2000). [hep-ex/0001015].

[21] C. McGrew, R. Becker-Szendy, C. B. Bratton, J. L. Breault, D. R. Cady, D. Casper, S. T. Dye, W. Gajewski *et al.*, Phys. Rev. **D59**, 052004 (1999).

[22] C. D. McGrew, "A Search for baryon nonconservation using the IMB-3 Detector," Ph. D. thesis, University of California at Irvine,. 1994.

[23] M. Claudson, M. B. Wise and L. J. Hall, Nucl. Phys. B **195**, 297 (1982).

[24] S. Aoki *et al.* [JLQCD Collaboration], Phys. Rev. **D62**, 014506 (2000). [hep-lat/9911026].

[25] Y. Suzuki *et al.* [TITAND Working Group Collaboration], [hep-ex/0110005].

[26] M. V. Diwan, R. L. Hahn, W. Marciano, B. Viren, R. Svoboda, W. Frati, K. Lande, A. K. Mann *et al.*, [hep-ex/0306053].

[27] A. Bueno, Z. Dai, Y. Ge, M. Laffranchi, A. J. Melgarejo, A. Meregaglia, S. Navas, A. Rubbia, JHEP **0704**, 041 (2007). [hep-ph/0701101].

[28] A. Birkedal, K. Matchev, M. Perelstein, Phys. Rev. **D70**, 077701 (2004). [hep-ph/0403004].

[29] M. Beltran, D. Hooper, E. W. Kolb, Z. A. C. Krusberg, T. M. P. Tait, JHEP **1009**, 037 (2010). [1002.4137 [hep-ph]].

[30] J. Goodman, M. Ibe, A. Rajaraman, W. Shepherd, T. M. P. Tait, H. -B. Yu, Phys. Lett. **B695**, 185-188 (2011). [1005.1286 [hep-ph]]; J. Goodman, M. Ibe, A. Rajaraman, W. Shepherd, T. M. P. Tait, H. -B. Yu, Phys. Rev. **D82**, 116010 (2010). [1008.1783 [hep-ph]].

[31] Y. Bai, P. J. Fox, R. Harnik, JHEP **1012**, 048 (2010). [1005.3797 [hep-ph]].

[32] P. J. Fox, R. Harnik, J. Kopp, Y. Tsai, [1103.0240 [hep-ph]].

[33] M. R. Buckley, [1104.1429 [hep-ph]].

[34] J. Pumplin, D. R. Stump, J. Huston, H. L. Lai, P. M. Nadolsky, W. K. Tung, JHEP **0207**, 012 (2002). [hep-ph/0201195].

[35] T. Aaltonen *et al.* [CDF Collaboration], Phys. Rev. Lett. **101**, 181602 (2008). [0807.3132 [hep-ex]].

[36] http://www-cdf.fnal.gov/physics/exotic/r2a/20070322.monojet/public/ykk.html

[37] L. Vacavant, I. Hinchliffe, J. Phys. G **G27**, 1839-1850 (2001).

[38] ATLAS Collaboration, ATLAS-CONF-2011-096 (2011).

[39] A. Rajaraman, W. Shepherd, T. M. P. Tait, A. M. Wijangco, [1108.1196 [hep-ph]].

[40] W. H. Press, D. N. Spergel, Astrophys. J. **296**, 679-684 (1985).

[41] K. Griest, D. Seckel, Nucl. Phys. **B283**, 681 (1987).

[42] A. Gould, Astrophys. J. **321**, 571 (1987).

[43] G. Angloher *et al.*, Astropart. Phys. **18**, 43 (2002).

[44] Z. Ahmed *et al.* [CDMS-II Collaboration], Phys. Rev. Lett. **106**, 131302 (2011). [1011.2482 [astro-ph.CO]].

[45] C. E. Aalseth *et al.* [CoGeNT Collaboration], Phys. Rev. Lett. **106**, 131301 (2011). [1002.4703 [astro-ph.CO]].

[46] G. Bertone, M. Fairbairn, Phys. Rev. **D77**, 043515 (2008). [0709.1485 [astro-ph]].

[47] A. Gould, Astrophys. J. **321**, 560 (1987).

[48] K. Hebeler, J. M. Lattimer, C. J. Pethick, A. Schwenk, Phys. Rev. Lett. **105**, 161102 (2010). [1007.1746 [nucl-th]].

[49] I. Goldman, S. Nussinov, Phys. Rev. **D40**, 3221-3230 (1989).

[50] C. Kouvaris, Phys. Rev. **D77**, 023006 (2008). [0708.2362 [astro-ph]]; C. Kouvaris, P. Tinyakov, Phys. Rev. **D82**, 063531 (2010). [1004.0586 [astro-ph.GA]].

[51] A. de Lavallaz, M. Fairbairn, Phys. Rev. **D81**, 123521 (2010). [1004.0629 [astro-ph.GA]].

[52] C. Kouvaris, P. Tinyakov, Phys. Rev. **D83**, 083512 (2011). [1012.2039 [astro-ph.HE]]; C. Kouvaris, P. Tinyakov, [1104.0382 [astro-ph.CO]].

[53] S. D. McDermott, H. -B. Yu, K. M. Zurek, [1103.5472 [hep-ph]].

[54] A. Gould, B. T. Draine, R. W. Romani, S. Nussinov, Phys. Lett. **B238**, 337 (1990).

[55] S. O. Kepler, S. J. Kleinman, A. Nitta, D. Koester, B. G. Castanheira, O. Giovannini, A. F. M. Costa, L. Althaus, Mon. Not. Roy. Astron. Soc. **375**, 1315-1324 (2007). [astro-ph/0612277].

[56] A. Bottino, G. Fiorentini, N. Fornengo, B. Ricci, S. Scopel, F. L. Villante, Phys. Rev. **D66**, 053005 (2002). [hep-ph/0206211].

[57] M. McCullough, M. Fairbairn, Phys. Rev. **D81**, 083520 (2010). [1001.2737 [hep-ph]].

[58] D. Hooper, D. Spolyar, A. Vallinotto, N. Y. Gnedin, Phys. Rev. **D81**, 103531 (2010). [1002.0005 [hep-ph]].

[59] D. Hooper, F. Petriello, K. M. Zurek, M. Kamionkowski, Phys. Rev. **D79**, 015010 (2009). [0808.2464 [hep-ph]].

[60] M. T. Frandsen, S. Sarkar, Phys. Rev. Lett. **105**, 011301 (2010). [1003.4505 [hep-ph]]; D. T. Cumberbatch, J. .A. Guzik, J. Silk, L. S. Watson, S. M. West, Phys. Rev. **D82**, 103503 (2010). [1005.5102 [astro-ph.SR]]; M. Taoso, F. Iocco, G. Meynet, G. Bertone, P. Eggenberger, Phys. Rev. **D82**, 083509 (2010). [1005.5711 [astro-ph.CO]]; J. Casanellas, I. Lopes, Mon. Not. Roy. Astron. Soc. **410**, 535-540 (2011). [1008.0646 [astro-ph.CO]]. I. Lopes, J. Silk, Astrophys. J. **722**, L95 (2010). [1009.5122 [astro-ph.SR]].

[61] R. Abbasi *et al.* [ICECUBE Collaboration], Phys. Rev. Lett. **102**, 201302 (2009). [0902.2460 [astro-ph.CO]].

[62] M. Fairbairn, P. Scott, J. Edsjo, Phys. Rev. **D77**, 047301 (2008). [0710.3396 [astro-ph]]; P. Scott, M. Fairbairn, J. Edsjo, Mon. Not. Roy. Astron. Soc. **394**, 82 (2008). [0809.1871 [astro-ph]].

[63] M. Pospelov, Phys. Rev. D **80**, 095002 (2009).

[64] J. D. Bjorken, R. Essig, P. Schuster and N. Toro, Phys. Rev. D **80**, 075018 (2009) [0906.0580 [hep-ph]].

[65] M. L. Graesser, I. M. Shoemaker, L. Vecchi, [1103.2771 [hep-ph]]; H. Iminniyaz, M. Drees, X. Chen, [1104.5548 [hep-ph]].

[66] M. Pospelov, A. Ritz and M. B. Voloshin, Phys. Lett. B **662**, 53 (2008).